Berra EF, Gaulton R, Barr S.

Commercial Off-the-Shelf Digital Cameras on Unmanned Aerial Vehicles for Multitemporal Monitoring of Vegetation Reflectance and NDVI.

***IEEE Transactions on Geoscience and Remote Sensing* 2017**

DOI: https://doi.org/10.1109/TGRS.2017.2655365

Commercial Off-The-Shelf Digital Cameras on Unmanned Aerial Vehicles for Multi-Temporal Monitoring of Vegetation Reflectance and NDVI

Abstract. This paper demonstrates the ability to generate quantitative remote sensing products by means of an Unmanned Aerial Vehicle (UAV) equipped with one unaltered and one near infrared-modified Commercial Off-The-Shelf (COTS) camera. Radiometrically calibrated orthomosaics were generated for 17 dates, from which digital numbers (DNs) were corrected to surface reflectance and to Normalized Difference Vegetation Index (NDVI). Validation against ground measurements showed that 84-90% of the variation in the ground reflectance and 95-96% of the variation in the ground NDVI could be explained by the UAV-retrieved reflectance and NDVI respectively. Comparisons against Landsat 8 data showed relationships of $0.73 \leq R^2 \geq 0.84$ for reflectance and $0.86 \leq R^2 \geq 0.89$ for NDVI. It was not possible to generate a fully consistent time series of reflectance, due to variable illumination conditions during acquisition on some dates. However, the calculation of NDVI resulted in a more stable UAV time series, which was consistent with a Landsat series of NDVI extracted over a deciduous and evergreen woodland. The results confirm that COTS cameras, following calibration, can yield accurate reflectance estimates (under stable within-flight illumination conditions), and that consistent NDVI time series can be acquired in very variable illumination conditions. Such methods have significant potential in providing flexible, low-cost approaches to vegetation monitoring at fine spatial resolution and for user-controlled revisit periods.

Keywords – Multispectral, phenology, Unmanned Aerial System, calibration, forest

1. INTRODUCTION

Recent advances in sensor and imaging technologies have led to Commercial off-the-shelf (COTS) digital cameras becoming an attractive option for aerial remote sensing due to their ease of use, low cost, compact size, low weight and compact data storage [1]. Coupled with an Unmanned Aerial Vehicle (UAV) to create an aerial imaging system, COTS cameras have provided very high spatial and temporal resolution data for applications in multiple different disciplines [1, 2].

COTS cameras can be used with off-the-shelf configurations (unaltered) or they can be modified to detect near infra-red radiation, once the hot mirror filter is removed [3], making it possible to design different camera systems for UAV-based remote sensing dependent on the type of images required. The combination of visible and near-infrared (NIR) wavelengths is particularly important in vegetation analysis due to the contrasting way that plant leaves reflect energy in this spectral range, behaviour which is the basis for many vegetation indices (VI), such as the widely used Normalized Difference Vegetation Index (NDVI) [4]. However, COTS cameras are not calibrated instruments and, for multispectral remote sensing applications, an approach needs to be identified to produce radiometrically consistent images from which spectral reflectance can be retrieved [5].

The data recorded by a camera`s sensor can be affected by a combination of effects coming from camera-related factors (vignetting effect, data storage, spectral response functions, exposure settings, post-processing steps) and environment-dependent factors (surface conditions, sun geometry, atmospheric effects, topographic effects) [2, 6]. These effects can diminish the capability to generate accurate quantitative information [6], which is critical in applications such

as quantification of land surface parameters or time series analysis [2]. The retrieval of surface spectral reflectance from COTS cameras needs therefore to take these factors into account.

Several studies have tested the potential of COTS cameras (at ground, UAV and airborne level) to create visible and NIR radiation images (using either a single or dual camera system), but without calibrating the images` digital numbers (DN) to physical units (e.g. reflectance) [2, 3, 7-9]. Comparatively, fewer studies have retrieved surface spectral reflectance from COTS cameras, and this has not always been from fully radiometrically calibrated images due to challenges in identifying all of the camera-related factors, such as the camera spectral sensitivities [10-12], vignetting effects [10, 12, 13] and data storage [8, 12]. In one study, Zaman *et al.* [5] proposed a workflow to retrieve reflectance from cameras on a UAV which took into account all the camera-related factors; the results looked consistent but were not validated. Therefore, better understanding of the quality of spectral data retrieved from COTS cameras is needed [12], especially for applications where consistent multi-temporal data sets are required, such as in agricultural and forest monitoring [1, 14] and satellite observation validation [15].

This paper tests the ability of two identical COTS cameras on-board a UAV to generate spectral reflectances and calibrated NDVI from hundreds of mosaicked images, for use in vegetation monitoring. To do so, a workflow was designed which brings together well known and standard methods for camera radiometric calibration in order to obtain a well calibrated and characterized reflectance product from COTS UAV sensors for consistent time-series generation. The unique contribution of this paper consists in the analysis of the outcomes of this process: 1) assessing the UAV-retrieved reflectance and NDVI against ground-measured reflectance and NDVI for a number of vegetation types (convolved to the UAV cameras and also to Landsat 8`s Operational Land Imager (L8-OLI) response functions); 2) assessing UAV-derived NDVI against

actual Landsat-derived reflectances and NDVI, a step which identified the best RGB channel of the NIR-modified camera to be used as the NIR band in the NDVI calculation; and 3) comparing two approaches for radiometric calibration of the data using empirical line methods and assessing the ability to generate a consistent time series of reflectance and NDVI for forest phenology applications.

2. METHODOLOGY

2.1. Ground and UAV data collection

The study area consists of c.15 ha of mixed deciduous and conifer woodland surrounded by agricultural fields, located in the northeast of England (55.219867°, -1.698661°). The main tree species are European larch (*Larix decidua*), Sycamore (*Acer pseudoplatanus*), Sessile oak (*Quercus petrea*), Sitka spruce (*Picea sitchensis*), Norway spruce (*Picea abies*) and English oak (*Quercus robur*). The area was flown weekly by one of two fixed-wing UAVs (Quest300 and QPOD - QuestUAV Ltd., Amble, UK) from March to June 2015, with one additional flight in February and one in August, totalling seventeen acquisition dates. The flights were carried out in diverse illumination conditions (due the nature of British weather) but around solar noon when possible. This study focuses primarily on a detailed dataset acquired on Day of Year (DOY) 111 (21/04/2015) providing full ground data for calibration, which was acquired under clear, sunny conditions.

The UAVs were flown on fully automated routes according to pre-programmed flight plans, which included a flying height of 122 m, acquisition of one image per 2.2 s and a 80% side-overlap. Two gimballed COTS Panasonic DMC-LX5 digital cameras (Panasonic UK Ltd., Bracknell,

Berkshire, UK) were used concurrently as imaging systems on-board on the UAVs. One Panasonic camera was left un-modified (VIS) and therefore sensitive to visible light; the second Panasonic was modified (MOD) to be sensitive to near NIR wavelengths. The modified camera was purchased pre-modified by the UAV manufacturer (QuestUAV Ltd., Amble, UK), and has had its hot mirror removed and replaced by an external long pass filter (unknown manufacturer, cut-off at 660 nm).

All UAV images were captured on manual settings (ISO-100, shutter speed 1/800 s, aperture f/2 and focus to infinity) and saved in RAW format. Ground Reflectance Calibration Targets (GCTs) were placed within the UAV survey's coverage on all the image acquisition dates for use in performing radiometric calibration (Section 2.5). These targets comprised of four lightweight wood boards measuring 1.2 x 1.2 x 0.01 m, which were painted black and three different grey tones with matt paint.

Measurements of relative reflectance were made in the field in order to apply the empirical line method for radiometric and atmospheric correction [16] and to validate the UAV-derived reflectance estimates. Spectral measurements were acquired of the four GCTs and diverse natural targets (22) with an ASD field spectrometer (FieldSpec Pro, ASD Inc., CO, U.S.), using an 8 degree fore optic accessory positioned at nadir, 1.5 m above the surface. A 24" white barium sulphate-based panel (LabSphere, Inc. NH, U.S.) was used as a white reference. Five spectral measurements were taken for each target. For the natural targets, the five measurements were made within a 1 m radius area with the central position surveyed with Real Time Kinematic (RTK) Global Navigation Satellite System (GNSS) method. The measurements were made on DOY 111 (straight after the UAV flights), due to the favourable weather conditions.

2.2. Spectral sensitivity determination

The Panasonic cameras` spectral sensitivities (Fig. 1) were measured using a monochromator, the methodology for which is available in Berra *et al.* [17]. The green channel of the visible camera showed the highest peak in response and a wide band width response, likely due to the Panasonic camera using a Bayer colour filter array [3]. The red channel of the modified camera was the most sensitive to NIR radiation, whereas the green and blue channels have a much lower peak response (both 0.47). The red and green channels have peak response within the red-edge feature of 700~720 nm [18], while the blue channel peaks within the NIR band, which is in accordance with what would be expected from a Bayer filter [7]. For comparison, the L8-OLI bands [19] have narrower response functions and don`t overlap, contrary to the Panasonic's Relative Spectral Response (RSR). The OLI Red band is positioned before and the OLI NIR band is positioned after the red-edge feature, wavelengths which maximize the spectral differences between green vegetation, therefore being ideal for NDVI calculations.

Enter Fig. 1

2.3. Vignetting correction

The vignetting effect on single images was determined by using the flat field approach [6, 20]. The flat field-based calibration of the Panasonic cameras was performed by taking 100 images of the interior surface a 0.5 m diameter integrating sphere (LabSphere, Inc. NH, U.S.) illuminated by four Quartz-Tungsten-Halogen lamps. The aperture and focus were the same as used during the field campaign, as these parameters modify the vignetting effect [20].

The images were acquired in RAW format and converted to dark-corrected linear TIFF images (Section 2.4). For each camera, an averaged flat field image for each RGB colour channel was calculated. A per-pixel correction factor look-up-table (LUT) was calculated [20] and its values were fitted by 8^{th} order polynomial models, resulting in a modelled LUT (Fig. 2).

All the RGB channels from both cameras presented a brightness attenuation away from the image centre, but the modified camera was most affected by vignetting (Fig. 2). The use of the modelled LUT values (Fig. 2) as multiplicative correction factors on individual images can therefore diminish the spatial nonuniformity of pixel intensities substantially.

Enter Fig. 2

2.4. UAV image corrections and generation of orthomosaics

The software DCRaw v9.25 (https://www.cybercom.net/~dcoffin/dcraw/dcraw.1.html) was used to linearly convert the RAW files into 16 bits TIFF images [17]. The effects of the dark current signal were corrected by subtracting a dark image from the RAW images [21].

The dark-corrected linear TIFF images were corrected for vignetting effects using the modelled LUT values (Section 2.3). The corrected images were thereafter mosaicked using the software Agisoft PhotoScan v.2 (Agisoft LLC, St. Petersburg, Russia). Orthomosaics were created individually per date and per camera following recommended settings [22], but with two modifications: 1) the dense point cloud was generated using the lowest reconstruction quality, as this produced orthomosaics with less artefacts over the forest area; 2) the orthomosaic was constructed with blending mode deactivated in order to preserve the original DN values. Five ground control points (GCPs) were used to generate georeferenced orthomosaics (5 cm spatial resolution). Six GCPs were used as check points, which revealed a 3D error of <8 cm for the VIS

and <11 cm for the MOD orthomosaics. This indicates that VIS and MOD orthomosaics can be combined/registered with a general accuracy of ±11 cm, i.e., ± 2.2 pixels.

2.5. Conversion to reflectance

2.5.1. Retrieving and validation of reflectance and NDVI

The empirical line method [16] was applied to retrieve surface reflectance from orthomosaic DNs of DOY 111 (reference date). The ASD measurements of relative spectral reflectance of GCTs and natural targets were corrected to absolute reflectance and convolved to the corresponding Panasonic-specific RSR curves using a MATLAB toolbox [23]. The field spectra were also convolved using the response functions of the L8-OLI sensor in order to compare how the Panasonic bands perform against this state-of-the-art sensor.

The GCTs were identified on the orthomosaics, from which the mean DN values were regressed against the convolved reflectance values, resulting in band-specific calibration coefficients to retrieve surface reflectance from the orthomosaic DNs. NDVI was also calculated, a step in which each MOD RGB band was combined with the VIS R band, in order to test which MOD channel would better perform as NIR band and also which MOD channel would best correlate with the OLI-derived NDVI.

A time series of L8-OLI and Landsat 7 Enhanced Thematic Mapper (L7-ETM+) surface reflectance products (processed according to [24, 25]) was extracted over the study area for the same period of time as the UAV flights. Six out of 15 images were selected, following exclusion of cloud contaminated images and L7-ETM+ images with data gaps (Scan Line Corrector-off). NDVI was calculated using the surface reflectance from the red and NIR bands.

The UAV-retrieved reflectance and NDVI were validated against the ASD ground measurements of reflectance and NDVI of 22 natural targets on DOY 111 and against L8-OLI reflectance and NDVI data (from DOY 113). The mean orthomosaic reflectance value was calculated from within a 1 m radius area, which coincided with the spectroradiometer measurement areas. The comparisons with L8-OLI were made over the area coinciding with the UAV orthomosaic limits (405 Landsat pixels, 36.45 ha). Each L8-OLI pixel value was compared to a mean orthomosaic value extracted from the area corresponding to each L8-OLI pixel. The accuracy of the results was assessed by analysis of scatter plots, R^2 and bias values.

2.5.2. Retrieving time series of reflectance/NDVI: application in forest phenology

Since the GCTs were present on every flight date, the empirical line method was applied through the entire time series to estimate reflectance and NDVI (as in Section 2.5.1). The same GCTs were used on 14 acquisition dates (from DOY 84 to 218) and standard equations were determined using the GCT ground reflectances as measured on DOY 111. However, different GCTs were tested during the first four acquisition dates (DOY 47, 56, 69 and 77), and equations for these days used the GCT reflectances as measured on DOY 77. Due to variable localised illumination conditions on some dates, it was not always possible to use the four GCTs as either one (DOY 106 and 133) or two (DOY 124) GCTs exhibited inconsistent illumination relative to the others. The GCTs ground reflectance was assumed to remain constant over time.

In addition to the standard approach to reflectance estimation, a simple new method was tested to produce consistent time series of NDVI. This consists of defining standard equations via the empirical line method on a reference date, forcing the constant to zero (equation C0), and then

applying these to the entire time series. This method aims to simplify the calibration procedure, as it reduces the need for GCTs in every field site data acquisition, making it easier to be implemented on an operational basis. This can be a major benefit for time series acquisitions or for surveying of large areas using UAVs, where VIs are required.

The hypothesis is that accurate calibration equations (with intercept zero), determined on a reference date, can be used to generate consistent time series of NDVI. This is expected due to the UAV images DNs being linearly related to measured surface reflectance, as shown here (R^2>0.99, RMSE<1.2%, Fig. 3) and elsewhere [10]. Therefore, if it is assumed that only changes in illumination condition affect the image DNs (linearly), and that if the red and NIR bands are consistent with each other, the normalized difference between red and NIR-retrieved surface reflectance (NDVI) will be significantly less affected by changes in illumination conditions, resulting in consistent NDVIs. However, the retrieved spectral reflectances are expected to be biased due to the illumination conditions being different from the reference date (Fig. 3), meaning that this approach is not suitable if reflectance data is needed.

The C0 approach assumes that the time series of UAV imagery will have the same atmospheric effects as for the reference date. However, it is known that the atmosphere conditions vary in time [26] and residual effects are expected in the NDVI because the red and NIR wavelengths are influenced differently by the atmosphere [27]. For satellite sensors, the atmosphere could reduce NDVI dynamics by as much as 10% [26, 28], but this is dependent of many factors, such as bandwidth and land cover type. These effects, however, can be expected to be smaller for UAV imagery, as low flying heights avoid strong interactions of ground reflected radiation with atmosphere (< 300 m, [29]) (122 m in this study).

Enter Fig. 3

Forcing the intercept from a reference equation to zero is necessary in order to avoid negative reflectances being calculated. For example (Fig. 3), the standard equation for MOD_B on DOY 111 (sunny) had an intercept of DN=1248; the standard equation for MOD_B on DOY 140 had an intercept of DN=598 and a steeper slope (cloudy conditions), which indicates that very low DNs (<1248) were recorded on DOY 140. If the standard equation from DOY 111 is applied to DOY 140, negative NIR reflectance and unrealistic NDVI values would be retrieved in those areas with DNs<1248. On the other hand, the C0 equation assures that positive (but biased) reflectance will be retrieved, allowing NDVI data to be calculated.

The effect of using the standard ($y = ax + b$, one different equation per band per date) and the C0 ($y = ax$, one single equation per band for the entire series) equations were investigated for four cases. First, the C0 equations were derived from the orthomosaics on DOY 111 and applied to the other orthomosaics (16 dates). The resulting time series of reflectance and NDVI was then compared against estimates obtained with the standard equations over a pasture area located 1 m from the GCTs, an area which was verified to have the same illumination conditions as the GCTs. The reflectance and NDVI retrieved by the standard equations can be considered true measurements and can be used as reference.

Second, C0 equations were derived from the orthomosaic on DOY 155 (cloudy day), and were used to retrieve reflectance and NDVI on the reference DOY 111. This allowed the estimates to be compared against the ASD ground measurements of 22 natural targets and against actual L8-OLI data (in a manner similar to Section 2.5.1).

Finally, a time series of UAV-derived reflectance and NDVI was retrieved using standard and C0 (from DOY 111) equations. The series was extracted over one sample area of evergreen (Sitka spruce) and one of deciduous (Larch) forest (L8-OLI pixel size), from which areas the mean values were calculated. The UAV temporal trends were analysed against each other and against a time series of Landsat data (L7-ETM+ and L8-OLI), which in turn allowed assessment of the potential of UAV acquired images to track the expected seasonal patterns (phenology) of this forest.

3. RESULTS

3.1. Validation of reflectance and NDVI on DOY 111

A linear relationship between convolved surface reflectance and orthomosaic DN over the GCTs was observed (R^2>0.99, RMSE<1.2%) (Fig. 3), which allowed the empirical line method to be applied. The results from the standard equations are analysed first.

The derived UAV-reflectances of natural targets were highly correlated with the ASD reflectances convolved to the Panasonics RSR ($0.84 \leq R^2 \geq 0.90$), with overestimation in the visible bands (<1%) and underestimation in the NIR bands (<1.5%) (Table 1). These small biases are the result of the data points being well distributed around the 1:1 line (Fig. 4). The comparisons with ASD reflectances convolved to L8-OLI RSR showed slightly lower R^2 for the VIS_R, VIS_G and MOD_R bands, whilst the other bands have the same R^2, with biases <1% in the visible bands and <11% in the NIR bands (Table 1). There were therefore only small differences between the reflectances convolved with the Panasonic cameras and L8-OLI RSRs in the visible bands, but more pronounced differences in the NIR bands, as OLI resulted in higher reflectance values than the MOD Panasonic. The convolution of a green vegetation spectra (Fig. 1) showed that the NIR-

modified Panasonic bands tended to estimate reflectances below the ASD values in the NIR or red-edge wavelengths, whilst the NIR band of OLI was able to simulate more precisely this reflectance.

The comparisons against actual L8-OLI reflectances showed moderate to strong relationships ($0.73 \leq R^2 \geq 0.84$) (Table 1). The analysis of the biases in UAV reflectance estimations showed that the direction was the same (except for the green band) and the magnitude was very similar to the comparisons between UAV and ASD convolved to L8-OLI.

Enter Table 1

Among the MOD-RGB channels, the MOD_B detected NIR reflectance in a way more similar to the L8-OLI NIR band (Fig. 4), with the highest R^2 and smallest bias (Table 1). This behaviour is as expected from the MOD RSRs, as the MOD_B has a higher sensitivity in the NIR and lower sensitivity in the red spectral region (Fig. 1). The UAV-derived NIR reflectances have a non-linear relationship with ASD measurements convolved to L8-OLI NIR RSR, especially for MOD_R (Fig. 4). For targets with high NIR reflectance, reflectance is underestimated by the UAV bands, due to the differing RSR functions.

Enter Fig. 4

The UAV-derived NDVIs were highly correlated with the NDVI calculated using ground measurements convolved to Panasonic ($0.95 \leq R^2 \geq 0.96$) and to L8-OLI ($0.93 \leq R^2 \geq 0.95$) RSR, with NDVI using MOD_B as NIR band achieving the highest R^2 and smallest bias (Table 1, Fig. 5). The UAV-derived NDVI was compared against actual Landsat NDVI data and the same benefits of using the MOD_B band were observed (Table 1, Fig. 5). These results indicate that the

NDVI calculated using MOD_B as the NIR band produces values closer to the traditional NDVI as calculated with the L8-OLI sensor.

Comparisons were also made with band-specific equations with the constant forced to zero, the results of which revealed the same R^2 as the standard equations in all data pairs analysed, i.e. UAV vs ASD and UAV vs L8-OLI imagery data (Table 1). The UAV-retrieved reflectances using the C0 equations yielded slightly higher values than the reflectances retrieved with the standard equations, especially for the NIR bands (Fig. 4). In terms of NDVI, the C0 equations resulted in either the same or slightly lower (0.01) R^2; the biases were consistently lower than the standard calibration equation (Table 1), resulting in the data points lying closer to the 1:1 line (Fig. 5).

Enter Fig. 5

3.2. Time series applied to forest phenology

The UAV reflectances retrieved using standard equations followed, in general, the pattern as detected by the Landsat sensors, but with some obvious 'spikes' (Fig. 6 a,b). These spikes were observed to occur on those dates when variable illumination led to a mixture of cloudy and sunny patches in the orthomosaics, with illumination conditions differing between imaging GCTs and vegetation targets. The calculation of NDVI diminished the effects of these abrupt variations in the UAV reflectance time series, resulting in a typical deciduous (Fig. 6 c) and evergreen (Fig. 6 d) NDVI temporal trend [30], similar to those from Landsat, and indicating that COTS cameras can be used to generate consistent vegetation index time-series data. However, the UAV NDVI time series still presented some date-to-date variations (mainly for the evergreen trees, Fig. 6 d), fluctuations that were not present in the Landsat series. The C0 equations resulted in less date-to-

date variation in the NDVI time series (Fig. 6 g,h), with both the NDVI data and the trend being very similar to the Landsat measurements.

Enter Fig. 6

The comparisons between the reflectances retrieved by the standard and C0 equations over the pasture sample revealed poor correlation in the VIS_R (R^2=0.26, RMSE=0.02, *n*=17) and no correlation in the MOD_B (R^2=0.01, RMSE=0.11, *n*=17) bands (Fig. 7). On the other hand, the NDVIs derived from the two methods presented very similar values through the time series (Fig. 7) and were strongly correlated with each other (R^2=0.97, RMSE=0.02, *n*=17). This supports the hypothesis that time series of NDVI could be retrieved based on a single calibration equation from a reference date, but date-specific (or illumination conditions-specific) equations are necessary if reflectance is needed.

Enter Fig. 7

In the second validation test, the UAV orthomosaic DNs from DOY 111 were converted to reflectance using C0 equations determined on DOY 155, with estimates compared against ASD and Landsat data (Table 2). The UAV-derived reflectances had the same R^2 as calculated in Table 1, but with significant higher biases (up to 80%). On the other hand, the NDVIs presented the same magnitude of biases, with the R^2 being either the same or just 0.01 lower than the values observed in Table 1, further confirming that NDVI could be adequately retrieved from a single C0 equation but single-band reflectance cannot.

Enter Table 2

4. DISCUSSION

4.1. Retrieving reflectance and NDVI from UAV COTS cameras

In this study two COTS cameras were radiometrically calibrated and their potential to be used as multispectral imaging systems was assessed. State-of-the-art equipment was used to accurately determine the vignetting effect and the spectral sensitivity of the COTS cameras. These camera-related characteristics are vital for spectral reflectance measurements, interpretation of the data and comparisons with other sensors.

In general, the correlation of UAV and ground spectral data was high; between 84-90% of the variation in the ground reflectance and 95-96% of the variation in the ground NDVI could be explained by the UAV-retrieved reflectance and NDVI, respectively. These results are similar to studies using scientific cameras (e.g. Tetracam) onboard on UAVs [31, 32] and confirm that COTS cameras, following calibration, can yield accurate reflectance and NDVI estimates. It would be valuable, in a future study, to conduct a direct comparison between scientific and COTS multispectral cameras to further assess the quality of COTS-acquired data.

Accurate reflectance estimates can be obtained even when orthomosaics consisted of hundreds of images acquired with COTS cameras, and when a single equation is used to retrieve reflectances based on GCTs appearing only on a single (or a few) images per acquisition. This can be explained, firstly, as a result of a consistent image pre-processing workflow, which generated orthomosaic DNs linearly related to ground reflectances; this indicates that the Panasonic sensors recorded radiance in a linear way and that the methodology used to correct the RAW images was able to preserve this relationship. Secondly, single images acquired with UAVs at low heights can present very strong variation in brightness values due to angular variation of reflectance

(bidirectional effect) [8, 11]. This effect can be potentially diminished if an orthomosaic is made of a dataset with high image overlap (>9 per point in this study), acquired within a short period of time (<15 min in this study). In this condition, processing algorithms can select the closest pixels to the nadir angle (among the overlapping images) to form the orthomosaic [22], resulting in orthomosaic pixels which could be assumed to have similar bidirectional effects, at least on flat areas.

Despite this assumption, there should still be some remaining influence of bidirectional effects in the orthomosaic DNs, which will account for some uncertainty in the retrieved reflectances. The calculation of NDVI is expected to account for some of these effects [33-36], which can explain the better performance of this index over the individual bands alone.

The blue channel from the modified camera was consistently the best candidate to be used as the NIR band either alone or in the NDVI calculation, in agreement with [37] but different from a number of alternative suggestions made in the literature [9, 10, 38]. Even though the MOD blue channel has lower sensitivity and lower SNR than the MOD red channel, it produces a stronger NIR response and consequent more useful and high quality data for vegetation monitoring. In future studies it may be beneficial to set a modified camera to have a higher exposure than the unmodified one, which would increase the blue channel sensitivity and SNR.

It is known that COTS cameras have the potential to be used as a multispectral sensor [10-12] but this should be done with care. The RGB response functions of a COTS camera are expected to be wide and overlapping, as shown here and elsewhere [17, 38], contrary to the narrow, well-defined and non-overlapping RSR present in satellite sensors [19]. This RSR overlapping can cause band correlation and a mixed spectral response [7]. However, by employing two cameras

simultaneously (one unmodified and one modified, as in this study) it is possible to acquire two spectrally separated bands, register them together and estimate VIs such as NDVI.

Alternatively, it is possible to use a single modified camera, where customized filters can allow either NIR-R-G [37] or NIR-G-B [18] images to be acquired. The Panasonic cameras (Fig. 1) could benefit from a NIR-R-G arrangement (for NDVI purposes), as the blue channel has a stronger NIR response. On the other hand, a NIR-G-B approach could be useful if red-edge-based indices are of interest, as the red channel has a strong peak response within the red-edge wavelengths. The great advantage of a single-camera approach is that the three bands are already registered, but this may bring some disadvantages, such as less control of the shape of the NIR band and no standard RGB colour images [1].

4.2. Time series from UAV COTS cameras

UAVs can be particularly helpful to obtain time-series data in regions that experience frequent cloud cover, such as Great Britain [39]. In our study area, only 6 cloud-free Landsat data sets were available, unevenly distributed in time, whilst UAV data were acquired 17 times on a weekly basis. Such temporal resolution can be particularly useful in phenology studies but also for critical situations such as monitoring plant disease or pest attacks [40].

The use of calibrated COTS cameras on a UAV allowed a consistent time series of NDVI to be obtained, although this was not always the case for the spectral reflectance. The acquisition of UAV data under cloudy conditions increases considerably the chance of obtaining high temporal resolution optical data, but it can result in difficulties in transforming image DNs to calibrated reflectance using the empirical line method, particularly in orthomosaics acquired during highly variable illumination conditions (patchy cloud), a problem which is also common to

other airborne data sets [41]. Further work on radiometric normalization of images [2] or cloud shadow detection and correction [42] could improve the results.

The calculation of NDVI significantly reduced the impact of varying illumination conditions and shadowing effects, an advantage also noted in other studies [33-36], and this highlights the importance of acquiring visible and NIR images concurrently. This resulted in a consistent time series of NDVI, allowing the expected temporal pattern of a deciduous and evergreen land cover [30] to be identified (Fig. 6 c,d).

A similar pattern could be inferred from the Landsat NDVI series (Fig. 6 c,d), but with a number of significant temporal gaps; a common problem with the Landsat series and other satellite sensors [43]. UAV-derived NDVI time series can be used therefore to identify seasonal transitions in vegetation activity with a more appropriate temporal resolution. UAV data can be also used to better understand the fine-scale spatial variability in phenology events occurring at a sub-pixel level for satellite data sets [30].

The calculation of NDVI using date-specific empirical line correction was not able to produce a totally noise-free time series (Fig. 6 c,d), and a simple new approach was observed to improve the results. The use of a single reference equation per band (with intercept zero), derived from a single date and applied across the whole time series, resulted in a more consistent time series of NDVIs (Fig. 6 g,h), highly comparable with the Landsat series. These results suggest that it may be sufficient to have GCTs for only one (or a small number of) reference dates and then apply a C0 equation from this date to the whole time series to calculate a series of NDVI values, which could improve the efficiency of data acquisition and processing. However, as our results

show, if estimates of spectral reflectance are necessary, rather than NDVI, date-specific (or illumination conditions-specific) calibration equations are clearly vital.

The noise present in the NDVI time series derived with the standard equations can be due to a few factors, which point towards the difficulty to determine well calibrated equations [16] in every acquisition date. First, it was not always possible to use the four GCTs on some dates as either one or two GCTs had different illumination conditions than the others; a fact which can increase the errors in the estimated reflectances [16]. Secondly, the GCTs were assumed to have a constant reflectance over time. In reality, the GCTs are not lambertian and, ideally, their reflectance should be measured in every date, which was impractical if not impossible on some occasions and would be costly and time consuming in operational contexts. This means that the calibration equations using GCTs` reflectance measured on a different date could be prone to added errors due to BRDF effects [44].

Finally, the standard equations can suffer uncertainties over very low DNs values, as the intercept value can be higher than the lowest DNs values within in the mosaics. In such a situation, unrealistic reflectance (and NDVI) values will be retrieved, particularly in heavily shadowed areas (due to trees or clouds shadows or a combination of both, intensified by high solar zenith angles). Forcing the constant to zero assumes therefore that all the bands, from both cameras, are perfectly consistent with each other, preventing unrealistic reflectance values being retrieved from low DNs values.

5. CONCLUSIONS

UAVs can acquire consistent fine spatial resolution data at user-controlled revisit periods, without the limitations that result from cloud presence. This represents a great flexibility over spaceborne optical systems, as vegetation changes can be monitored at a higher temporal resolution.

Broad-band surface reflectance and NDVI for vegetated areas can be retrieved with confidence from orthomosaics generated from calibrated COTS cameras onboard a UAV. It was not entirely possible in this study to generate a consistent time series of reflectance, due to variable illumination conditions during acquisitions on some dates, although further work on normalizing single images could improve the results. On the other hand, the calculation of NDVI, using the blue channel from a modified camera as NIR band, resulted in a stable time series. A more consistent NDVI time series was generated from radiometric calibration equations which have had their constants forced to zero and were based on single date GCTs, as NDVI adequately adjusts for variation in the acquisition conditions.

6. ACKNOWLEDGEMENT

E. Berra would like to thank Science without Borders Brazil (grant 1121/13-8) for funding this work as part of his PhD. We would also like to thank: Dr Gary Llewellyn from the Natural Environment Research Council (NERC) Airborne Research and Survey Facility (ARSF) for assistance with the vignetting correction; Dr Christopher MacLellan, Dr Alasdair MacArthur (from the NERC Field Spectroscopy Facility - NERC FSF) and Simon Gibson-Poole for assistance with the camera spectral sensitivity determination, and Maria Peppa, Magdalena Smigaj and Martin Robertson for their substantial help with the UAV data collection.

7. REFERENCES

[1] G. Rabatel, N. Gorretta, and S. Labbe, "Getting simultaneous red and near-infrared band data from a single digital camera for plant monitoring applications: Theoretical and practical study," *Biosys. Eng.*, vol. 117, pp. 2-14, Jan. 2014.

[2] V. Lebourgeois, A. Bégué, S. Labbé, B. Mallavan, L. Prévot, and B. Roux, "Can commercial digital cameras be used as multispectral sensors? A crop monitoring test," *Sensors*, vol. 8, no. 11, pp. 7300-7322, 2008.

[3] G. J. Verhoeven, P. F. Smet, D. Poelman, and F. Vermeulen, "Spectral characterization of a digital still camera's nir modification to enhance archaeological observation," *IEEE Trans. Geosci. Remote Sens.*, vol. 47, no. 10, pp. 3456-3468, Oct. 2009.

[4] J. W. Rouse, R. H. Haas, J. A. Schell, and D. W. Deering, "Monitoring vegetation systems in the great plains with erts," in *Proc. Third ERTS Symposium*, Washington. D.C., 1973, pp. 309-317.

[5] B. Zaman, A. Jensen, S. R. Clemens, and M. McKee, "Retrieval of spectral reflectance of high resolution multispectral imagery acquired with an autonomous unmanned aerial vehicle: Aggieair™," *Photogr. Engin. Remote Sens.*, vol. 80, no. 12, pp. 1139-1150, Jan. 2014.

[6] J. Kelcey, and A. Lucieer, "Sensor correction of a 6-band multispectral imaging sensor for uav remote sensing," *Remote Sens.*, vol. 4, no. 5, pp. 1462-1493, 2012.

[7] W. Nijland, R. de Jong, S. M. de Jong, M. A. Wulder, C. W. Bater, and N. C. Coops, "Monitoring plant condition and phenology using infrared sensitive consumer grade digital cameras," *Agricult. Forest Meteor.*, vol. 184, pp. 98-106, 2014.

[8] J. Rasmussen, G. Ntakos, J. Nielsen, J. Svensgaard, R. N. Poulsen, and S. Christensen, "Are vegetation indices derived from consumer-grade cameras mounted on uavs sufficiently reliable for assessing experimental plots?," *Europ. Journ. Agron.*, vol. 74, pp. 75-92, Mar. 2016.

[9] C. Yang, J. Westbrook, C. Suh, D. Martin, W. Hoffmann, Y. Lan, B. Fritz, and J. Goolsby, "An airborne multispectral imaging system based on two consumer-grade cameras for agricultural remote sensing," *Remote Sens.*, vol. 6, no. 6, pp. 5257-5278, 2014.

[10] A. J. Mathews, "A practical uav remote sensing methodology to generate multispectral orthophotos for vineyards: Estimation of spectral reflectance using compact digital cameras," *Intern. J. Appl. Geosp. Resear.*, vol. 6, no. 4, pp. 65-87, 2015.

[11] T. Hakala, J. Suomalainen, and J. I. Peltoniemi, "Acquisition of bidirectional reflectance factor dataset using a micro unmanned aerial vehicle and a consumer camera," *Remote Sens.*, vol. 2, no. 3, pp. 819-832, 2010.

[12] S. K. von Bueren, A. Burkart, A. Hueni, U. Rascher, M. P. Tuohy, and I. J. Yule, "Deploying four optical uav-based sensors over grassland: Challenges and limitations," *Biogeosc.*, vol. 12, no. 1, pp. 163-175, 2015.

[13] C. Wang, and S. W. Myint, "A simplified empirical line method of radiometric calibration for small unmanned aircraft systems-based remote sensing," *IEEE J. Sel. Topics Appl. Earth Observ. Remote Sens.*, vol. 8, no. 5, pp. 1876-1885, May. 2015.

[14] H. S. Yun, S. H. Park, H.-J. Kim, W. D. Lee, K. D. Lee, S. Y. Hong, and G. H. Jung, "Use of unmanned aerial vehicle for multi-temporal monitoring of soybean vegetation fraction," *J. Biosyst. Eng.*, vol. 41, no. 2, pp. 126-137, 2016.

[15] Y. Honda, K. Kajiwara, R. Sharma, A. Ono, K. Imaoka, H. Murakami, M. Hori, Y. Ono, and D. Rostand, "Land validation for gcom-c1/sgli using uav," *Sensors, systems, and next-generation satellites xvi*, *Proc.* Of spie R. Meynart, S. P. Neeck and H. Shimoda, eds., Bellingham: SPIE, 2012.

[16] G. M. Smith, and E. J. Milton, "The use of the empirical line method to calibrate remotely sensed data to reflectance," *Int. J. Remote Sens.,* vol. 20, no. 13, pp. 2653-2662, 1999.

[17] E. Berra, S. Gibson-Poole, A. MacArthur, R. Gaulton, and A. Hamilton, "Estimation of the spectral sensitivity functions of un-modified and modified commercial off-the-shelf digital cameras to enable their use as a multispectral imaging system for uavs," *Int. Arch. Photogramm. Remote Sens. Spatial Inf. Sci.,* vol. XL-1/W4, pp. 207-214, 2015.

[18] E. R. Hunt, Jr., W. D. Hively, S. J. Fujikawa, D. S. Linden, C. S. T. Daughtry, and G. W. McCarty, "Acquisition of nir-green-blue digital photographs from unmanned aircraft for crop monitoring," *Remote Sens.,* vol. 2, no. 1, pp. 290-305, Jan. 2010.

[19] J. Barsi, K. Lee, G. Kvaran, B. Markham, and J. Pedelty, "The spectral response of the landsat-8 operational land imager," *Remote Sens.,* vol. 6, no. 10, pp. 10232, 2014.

[20] W. Yu, "Practical anti-vignetting methods for digital cameras," *IEEE Trans. Cons. Electr.,* vol. 50, no. 4, pp. 975-983, Nov. 2004.

[21] J. Suomalainen, N. Anders, S. Iqbal, G. Roerink, J. Franke, P. Wenting, D. Hünniger, H. Bartholomeus, R. Becker, and L. Kooistra, "A lightweight hyperspectral mapping system and photogrammetric processing chain for unmanned aerial vehicles," *Remote Sens.,* vol. 6, no. 11, pp. 11013, 2014.

[22] AgiSoft, "Agisoft photoscan user manual: Professional edition, version 1.2," 2015, p. 103.

[23] I. Robinson, and A. MacArthur, "The field spectroscopy facility post processing toolbox user guide," *Post processing spectral data in MATLAB,* Natural Environment Research Council, 2011.

[24] USGS, "Landsat 4-7 climate data record (cdr) surface reflectance," *Product guide,* U.S. Geological Survey, 2016, p. 27.

[25] USGS, "Provisional landsat 8 surface reflectance code (lasrc) product," *Product guide,* U.S. Geological Survey, 2016, p. 27.

[26] J. R. Nagol, E. F. Vermote, and S. D. Prince, "Effects of atmospheric variation on avhrr ndvi data," *Remote Sens. Environ.,* vol. 113, no. 2, pp. 392-397, 2009.

[27] R. B. Myneni, and G. Asrar, "Atmospheric effects and spectral vegetation indexes," *Remote Sens. Environ.,* vol. 47, no. 3, pp. 390-402, Mar. 1994.

[28] J. Qi, Y. Kerr, and A. Chehbouni, "External factor consideration in vegetation index development," in *Proc. Sixth International Colloquium on Physical Measurements and Signatures in Remote Sensing*, Val d'Isère, France 1994, pp. 723-730.

[29] M. Herrero-Huerta, D. Hernández-López, P. Rodriguez-Gonzalvez, D. González-Aguilera, and J. González-Piqueras, "Vicarious radiometric calibration of a multispectral sensor from an aerial trike applied to precision agriculture," *Comput. Electron. Agric.,* vol. 108, pp. 28-38, 2014.

[30] G. Hmimina, E. Dufrêne, J. Y. Pontailler, N. Delpierre, M. Aubinet, B. Caquet, A. de Grandcourt, B. Burban, C. Flechard, and A. Granier, "Evaluation of the potential of modis satellite data to predict vegetation phenology in different biomes: An investigation using ground-based ndvi measurements," *Remote Sens. Environ.,* vol. 132, pp. 145-158, 2013.

[31] J. A. J. Berni, P. J. Zarco-Tejada, L. Suarez, and E. Fereres, "Thermal and narrowband multispectral remote sensing for vegetation monitoring from an unmanned aerial vehicle," *IEEE Trans. Geosci. Remote Sens.,* vol. 47, no. 3, pp. 722-738, Mar. 2009.

[32] A. S. Laliberte, M. A. Goforth, C. M. Steele, and A. Rango, "Multispectral remote sensing from unmanned aircraft: Image processing workflows and applications for rangeland environments," *Remote Sens.,* vol. 3, no. 11, pp. 2529-2551, 2011.

[33] B. Matsushita, W. Yang, J. Chen, Y. Onda, and G. Qiu, "Sensitivity of the enhanced vegetation index (evi) and normalized difference vegetation index (ndvi) to topographic effects: A case study in high-density cypress forest," *Sensors,* vol. 7, no. 11, pp. 2636-2651, 2007.

[34] G. Samseemoung, P. Soni, H. P. W. Jayasuriya, and V. M. Salokhe, "Application of low altitude remote sensing (lars) platform for monitoring crop growth and weed infestation in a soybean plantation," *Prec. Agri.,* vol. 13, no. 6, pp. 611-627, 2012.

[35] S. G. Bajwa, and L. Tian, "Multispectral cir image calibration for cloud shadow and soil background influence using intensity normalization," *Appl. Eng. Agric.,* vol. 18, no. 5, pp. 627, 2002.

[36] A. Shahtahmassebi, N. Yang, K. Wang, N. Moore, and Z. Shen, "Review of shadow detection and de-shadowing methods in remote sensing," *Chinese Geogr. Scien.,* vol. 23, no. 4, pp. 403-420, 2013.

[37] G. J. Verhoeven, "Near-infrared aerial crop mark archaeology: From its historical use to current digital implementations," *J. Archaeol. Method Theory,* vol. 19, no. 1, pp. 132-160, Mar. 2012.

[38] P. M. Dare, "Small format digital sensors for aerial imaging applications," in *Proc. XXI ISPRS Congress*, Beijing, 2008, pp. 533 - 538.

[39] R. P. Armitage, F. Alberto Ramirez, F. Mark Danson, and E. Y. Ogunbadewa, "Probability of cloud-free observation conditions across great britain estimated using modis cloud mask," *Remote Sens. Lett.*, vol. 4, no. 5, pp. 427-435, Jan. 2013.

[40] F. A. Vega, F. C. Ramírez, M. P. Saiz, and F. O. Rosúa, "Multi-temporal imaging using an unmanned aerial vehicle for monitoring a sunflower crop," *Biosys. Eng.*, vol. 132, pp. 19-27, 2015.

[41] A. S. Hope, K. R. Pence, and D. A. Stow, "Ndvi from low altitude aircraft and composited noaa avhrr data for scaling arctic ecosystem fluxes," *Int. J. Remote Sens.*, vol. 25, no. 20, pp. 4237-4250, Jan. 2004.

[42] E. Bondi, C. Salvaggio, M. Montanaro, and A. D. Gerace, "Calibration of uas imagery inside and outside of shadows for improved vegetation index computation," in *Proc. SPIE Commercial and Scientific Sensing and Imaging*, Maryland, US, 2016, pp. 98660J: 1-7.

[43] J. I. Fisher, J. F. Mustard, and M. A. Vadeboncoeur, "Green leaf phenology at landsat resolution: Scaling from the field to the satellite," *Remote Sens. Environ.*, vol. 100, no. 2, pp. 265-279, 2006.

[44] S. R. Sandmeier, and K. I. Itten, "A field goniometer system (figos) for acquisition of hyperspectral brdf data," *IEEE Trans. Geosci. Remote Sens.*, vol. 37, no. 2, pp. 978-986, Mar. 1999.

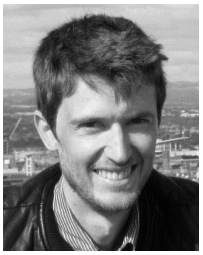

Elias F. Berra received the B.A. degree in forest engineering from the Federal University of Santa Maria, Brazil, in 2010 and the master`s degree in remote sensing from the Federal University of Porto Alegre, Brazil, in 2013.

He is currently a Ph.D. student in geomatics at Newcastle University, UK. His research is focused on monitoring of forest phenology with aid of digital cameras onboard drones.

Rachel Gaulton received the Ph.D. degree in geosciences, specialized in airborne remote sensing for forestry, from the University of Edinburgh, Edinburgh, UK, in 2009.

She is currently a lecturer in the School of Civil Engineering and Geosciences, Newcastle University, UK. Her research interests are focussed on the development of multi-scale and multi-platform remote sensing approaches for vegetation monitoring.

Stuart Barr received a Ph.D. degree in Urban earth observation from the University of Wales Swansea, UK, in 2002.

He is a senior lecturer in Geographical Information Science in the School of Civil Engineering and Geosciences, Newcastle University, UK. His research interests include the use of multi-source remote sensing and geospatial data for environmental risk analysis.

FIGURES AND TABLES

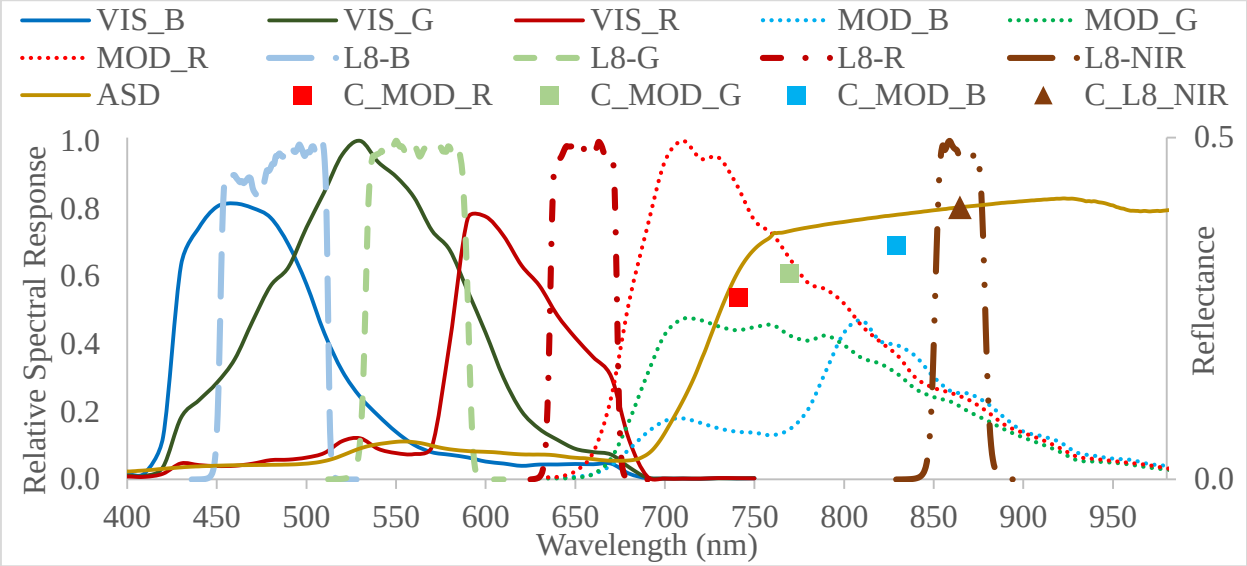

Fig. 1. Relative spectral response of the unmodified (VIS) and modified (MOD) Panasonic cameras for the red (R), green (G) and blue (B) channels. The Landsat 8`s OLI (L8) band sensitivities are also shown for comparison purposes. The reflectance curve of a grass target (ASD) represents a typical reflectance curve of green vegetation cover, the values of which were convolved (C) using the RGB MOD and L8 NIR bands.

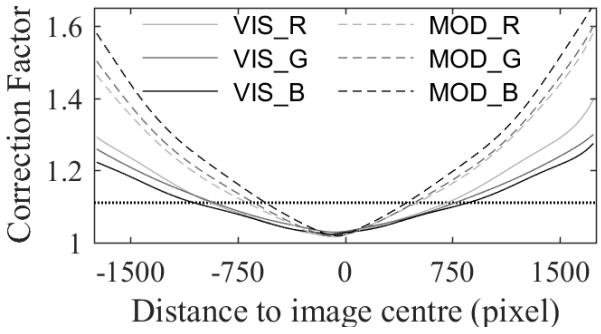

Fig. 2. Modelled vignetting effect (correction factors) for the RGB channels of the unmodified (VIS) and modified (MOD) Panasonic cameras. The solid horizontal line indicates a loss of brightness intensity of 10%.

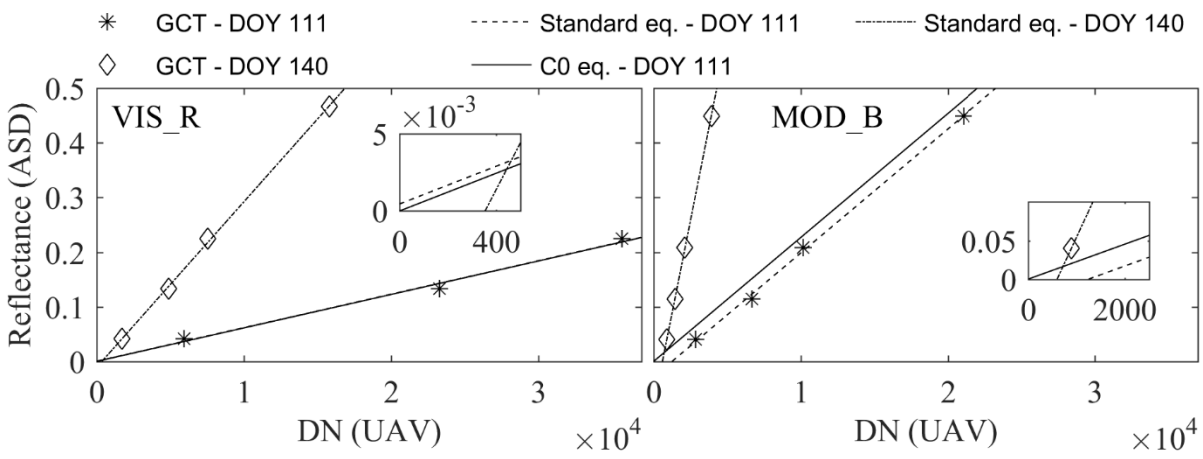

Fig. 3. Relationship between ground reflectance and UAV orthomosaic DNs over four ground calibration targets (GCTs) for the red channel of the visible camera (VIS_R) and blue channel of the NIR-modified camera (MOD_B). Standard equations on DOY 111 have had their constant set to zero (C0 eq.). Inset enlarged graphs within each graph are included in order to better show the intercepts.

Table 1. R^2 and bias (in brackets) values from comparison of reference (ASD, convolved to both Panasonics and L8-OLI RSR) and actual Landsat observations (L8-OLI imagery)) with UAV-derived reflectances and NDVIs. NDVIs were calculated using the MOD_R ($NDVI_R$), MOD_G ($NDVI_G$) and MOD_B ($NDVI_B$) as NIR band. The standard equations (y = ax + b) were also tested with their constant forced to zero (y = ax), based on the reference DOY 111.

	UAV vs ASD (*n*=22)[1]				UAV vs L8-OLI imagery (*n*=405)[2]	
	Panasonic RSR		L8-OLI RSR			
	y = ax + b	y = ax	y = ax + b	y = ax	y = ax + b	y = ax
VIS_R	0.86(0.009)	0.86(0.009)	0.85(0.009)	0.85(0.008)	0.83(0.007)	0.83(0.006)
VIS_G	0.84(0.009)	0.84(0.001)	0.82(-0.004)	0.82(-0.012)	0.83(-0.002)	0.83(-0.009)
VIS_B	0.87(0.007)	0.87(0.006)	0.87(0.010)	0.87(0.010)	0.84(0.008)	0.84(0.008)
MOD_R	0.85(-0.010)	0.85(0.007)	0.83(-0.103)	0.83(-0.086)	0.73(-0.100)	0.73(-0.082)
MOD_G	0.88(-0.012)	0.88(0.009)	0.88(-0.080)	0.88(-0.059)	0.77(-0.081)	0.77(-0.060)
MOD_B	0.90(-0.013)	0.90(0.015)	0.90(-0.052)	0.90(-0.024)	0.80(-0.058)	0.80(-0.030)
$NDVI_R$	0.95(-0.057)	0.95(-0.024)	0.93(-0.133)	0.93(-0.100)	0.86(-0.162)	0.86(-0.123)
$NDVI_G$	0.96(-0.056)	0.95(-0.021)	0.95(-0.107)	0.94(-0.072)	0.88(-0.131)	0.87(-0.092)
$NDVI_B$	0.96(-0.053)	0.95(-0.012)	0.95(-0.079)	0.94(-0.038)	0.89(-0.098)	0.88(-0.055)

[1]Comparisons made over natural ground targets; [2]Comparisons made over the whole forest area and its surroundings.

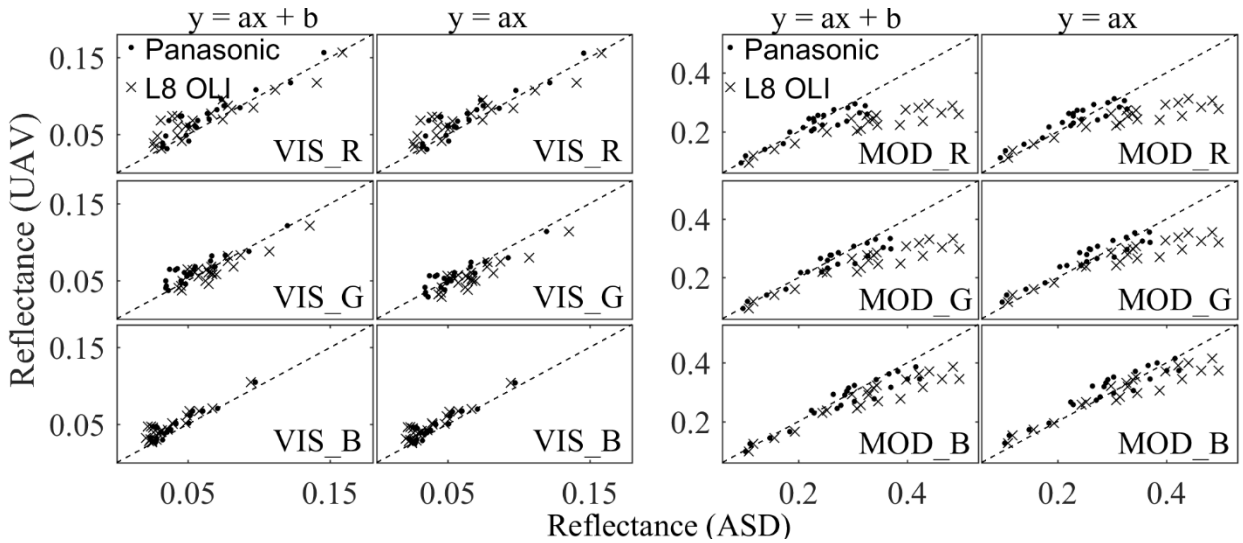

Fig. 4. Comparison of reference (ASD, convolved to Panasonic cameras and L8-OLI RSR) and retrieved reflectance (UAV) over 22 natural targets. The original equations (y = ax + b) were also tested with their constant forced to zero (y = ax). The dashed line shows the 1:1 relationships.

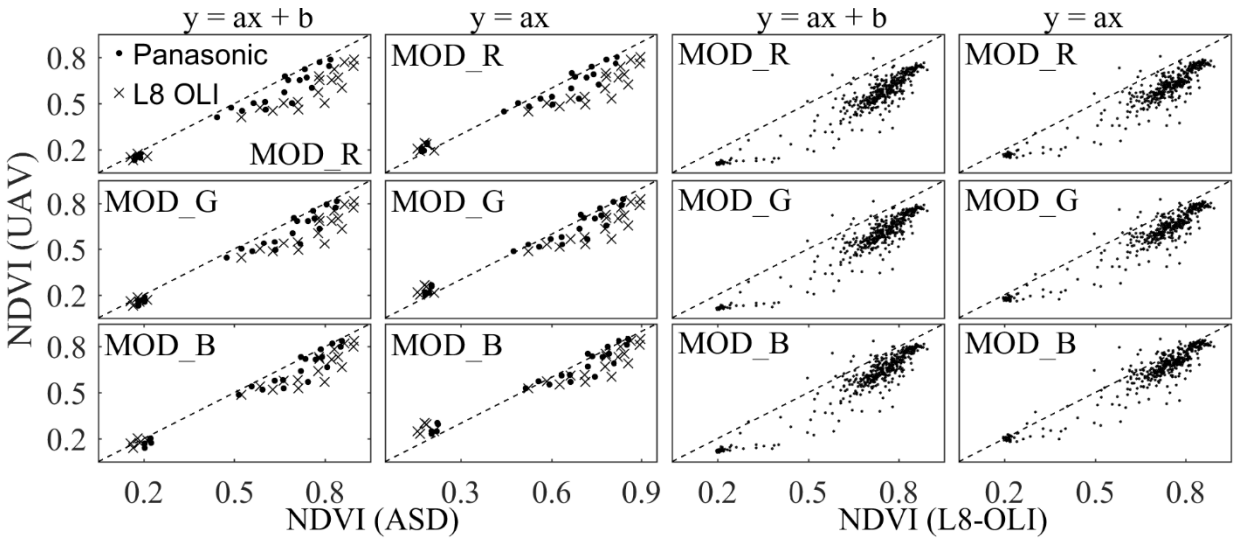

Fig. 5. UAV-derived NDVI are compared against ASD-derived NDVI, over ground natural targets (convolved to Panasonic and L8-OLI RSR) (1st and 2nd column, *n*=22) and against actual L8-OLI data, over the whole woodland and its surroundings (3rd and 4th column, *n*=405). NDVI (UAV) was calculated using the VIS_R channel as red band and the three MOD channels as NIR band. Standard equations are represented by "y = ax + b" and equations with no intercept are "y = ax". The dashed line shows the 1:1 relationships.

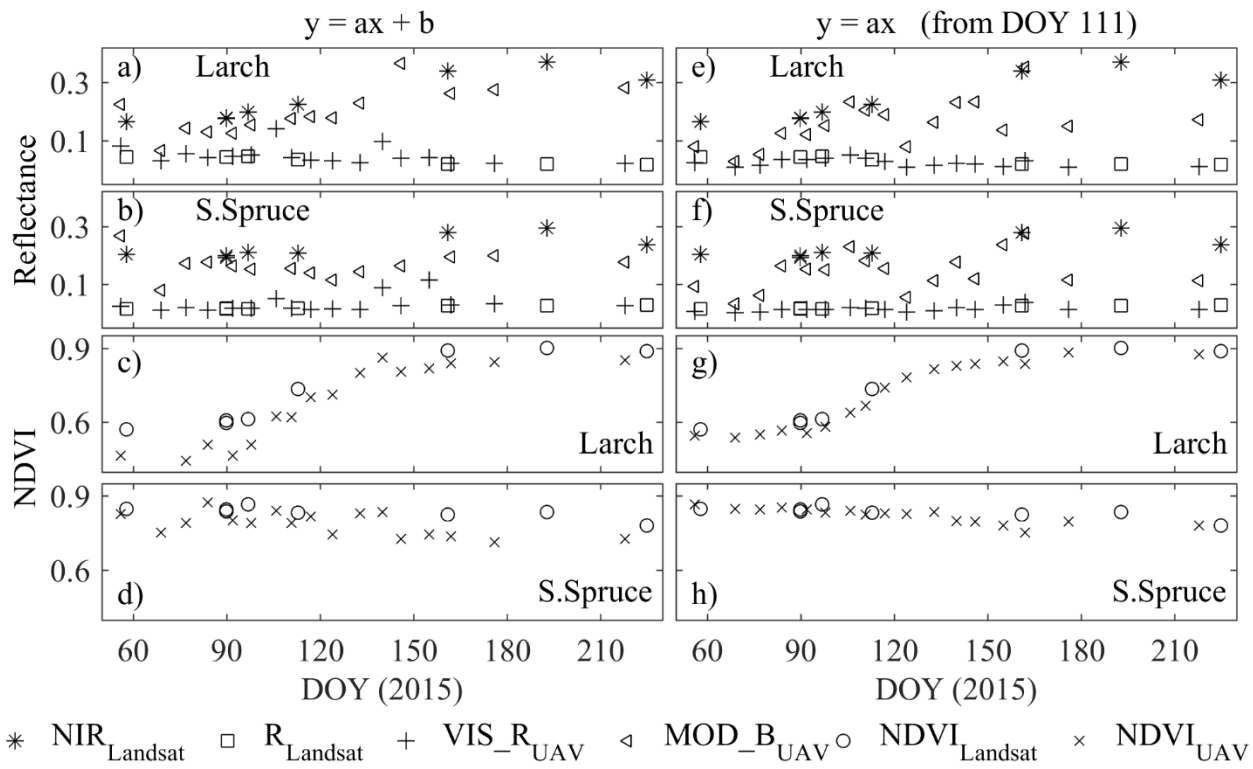

Fig. 6. Time series of reflectance and NDVI from UAV and Landsat sensors. The UAV reflectances were retrieved via empirical line methods using either one specific equation per day (standard equations) (a-d) or one single equation (C0 equations) from the reference DOY 111 (e-h).

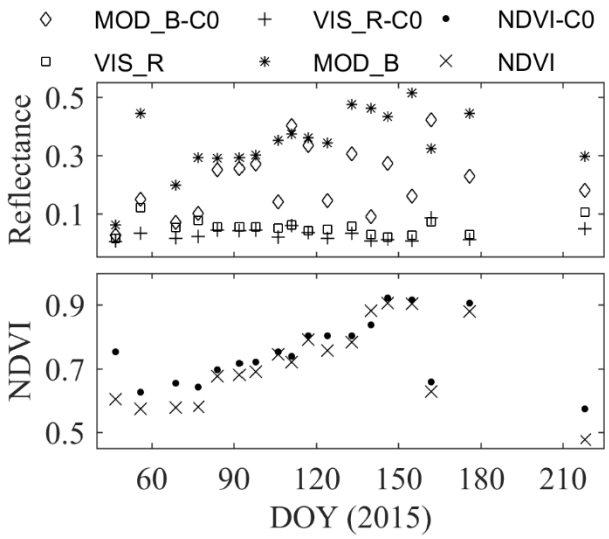

Fig. 7. Comparison between UAV spectral data retrieved using one different equation per day and one single equation from DOY 111 (indicated as C0) over a pasture sample located 1 m from the GCTs.

Table 2. R^2 and bias (in brackets) values between measured (ASD, convolved to both Panasonics and L8-OLI RSR) and estimated (UAV) reflectances and NDVIs on DOY 111. An equation from DOY 155 with constant zero (y = ax) was used to estimate the UAV spectral data on DOY 111.

	UAV vs ASD (n=22)[1]		UAV vs L8-OLI imagery (n=403)[2]
	Panasonic RSR	L8-OLI RSR	
VIS_R	0.86(0.22)	0.85(0.22)	0.83(0.173)
VIS_G	0.84(0.18)	0.82(0.16)	0.83(0.125)
VIS_B	0.87(0.12)	0.87(0.12)	0.84(0.093)
MOD_R	0.85(-0.67)	0.83(0.57)	0.73(0.435)
MOD_G	0.88(-0.72)	0.88(0.65)	0.77(0.503)
MOD_B	0.90(0.78)	0.90(0.75)	0.80(0.592)
$NDVI_R$	0.94(-0.052)	0.93(-0.128)	0.86(-0.149)
$NDVI_G$	0.95(-0.053)	0.94(-0.104)	0.87(-0.122)
$NDVI_B$	0.95(-0.051)	0.94(-0.076)	0.88(-0.091)

[1]Comparisons made over natural ground targets; [2]Comparisons made over the whole forest area and its surroundings.